# Chapter 4

# Optical separation of $H_2$POSD enantiomers

In this chapter, quantum simulations for the optical separation of enantiomers will be presented. The model system will be introduced in section 4.1 together with the criteria for the selection of this model. Previous work for such model system with emphasis in converting one enantiomer to the other will be outlined in section 4.1.1. The employed coordinates and their justification will be discussed in section 4.2. Section 4.3 shows the equilibrium geometry of the $H_2$POSH molecular system. In section 4.4, the 2D-Hamiltonian will be discussed. In section 4.5, the potential energy surfaces and the dipole moments are shown. After constructing the potential energy surfaces and the Hamiltonian, the ground state vibrational eigenfunctions and eigenvalues are calculated and discussed in section 4.6. Finally, the design of the laser pulse strategy to separate $H_2$POSD enantiomers in an oriented racemate will be presented in section 4.7.

## 4.1 Model system

The selection of a suitable model system is a very important step in the simulation of optical separation of enantiomers. Several criteria should be fulfilled for this purpose [181, 182]:

a) The molecule should be small enough to be investigated by accurate quantum mechanical and quantum dynamical methods.

b) For the sake of simplicity, the model system should possess one source of molecular chirality, otherwise the molecule will have more than two stereoisomers.

c) Preferably, the reaction of interconversion of enantiomers should be simple to avoid other complicated side reactions.
d) The potential energy surface must possess two minima separated by a barrier height, which should be high and broad enough to prevent immediate tunneling from one enantiomer to the other, see Fig. 4.1.

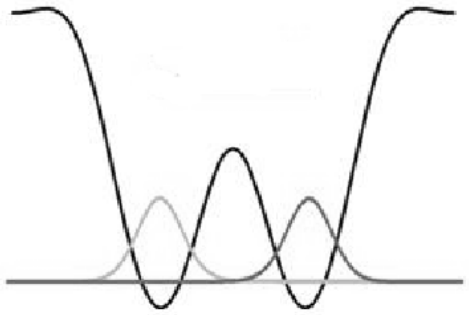

Figure 4.1: Schematic double well potential energy curve that represents two enantiomers separated by a potential barrier

e) The life time of each enantiomer must be much longer than the laser field duration, otherwise, after the preparation of an enantiomer, this might be converted to the other one right after the laser field application.
f) The molecular transition dipole moment should couple strongly with the laser field to avoid intense laser fields which might result in photo-ionization or other undesired processes, which would damage the system. If the coupling is weak - the transition dipole moment components are small - one has to repeat the laser pulse sequence to get complete conversion of one enantiomer to the other. In this case, the total employed time should be much smaller than the life time of one enantiomer (see e)).
g) The employed laser pulses should be available experimentally.

Deuterated phosphinothioic acid, $H_2POSD$, has been chosen as a suitable model system, see Fig. 4.2.

This molecule possesses axial chirality and it has two stable isomers (atropisomers) at ambient temperature. Each enantiomer is converted to the other by a torsional rotation of the S-D around the P-S bond keeping the $H_2PO$ fragment frozen. The obtained enantiomers are shown in Figure 4.3.

The $H_2POSD$ model fulfills the above criteria since: a) It is a small molecule and it can be studied using high level quantum chemical calculations, b) It con-

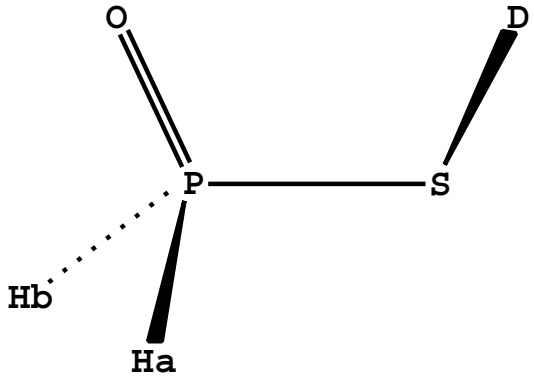


Figure 4.2: The model system $H_2POSD$

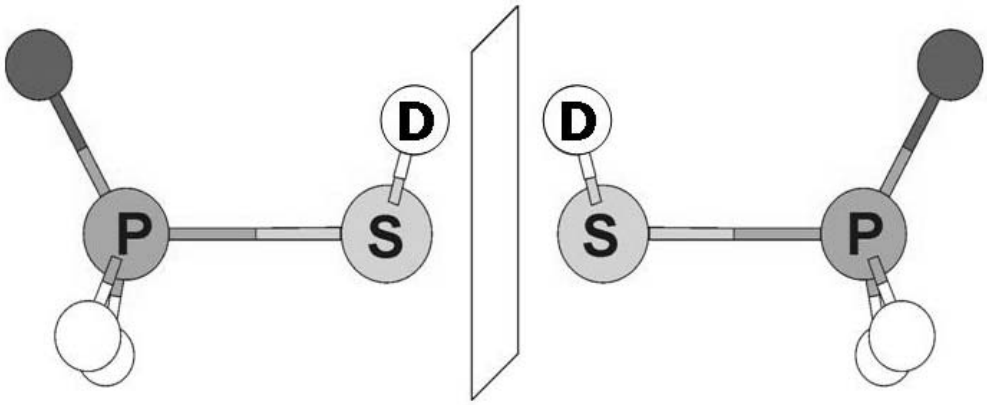


Figure 4.3: The enantiomers of the $H_2POSD$ model system

sists of two enantiomers connected by one source of molecular chirality, c) As a first approximation, the conversion between the two enantiomers takes place by only one degree of freedom, i.e. a torsional rotation, which makes the study of the molecular chirality relatively simple, d) The potential energy surface consists of two minima separated by a barrier which is high enough to stabilize one enantiomer during the considered time scale, as shown in Figure 4.1, e) The life time of each enantiomer is long in the context of a femtosecond time domain, see section 4.7. f) The molecule's transition dipole moment represents a moderate coupling with the laser field, for more details see section 4.7. g) The proposed laser strategy can be implemented experimentally for chiral molecules [2].

### 4.1.1 Review of the previous work

### 4.1.2 Laser control to asymmetric synthesis

Laser control of chemical reactions has been established experimentally since the first pump-probe experiment by Zewail [183, 184]. Theoretically, by means of coherent control Shapiro, Brumer and coworkers have suggested to use linearly polarized laser pulses to control molecular chirality. In their first attempt, in 1991, they considered a molecule of the type ABC and with $C_s$ symmetry. This molecule can be photo-dissociated into AB + C or A + BC by means of laser pulses where the four species are all chiral [79]. Later on, they simulate enantioselection from a racemic mixture using a model system with a double well electronic ground state potential and a single well electronic excited state potential. They used a four level simulation with the two enantiomers in the electronic ground state and the other two levels are in the excited states with different symmetries [185]. Furthermore, Shapiro and coworkers proposed that achiral light can encode quantum coherences leading to enantiomeric excess. This procedure can be repeated successively, in the so-called laser distillation fashion [80].

The quantum simulations of selective preparation of enantiomers using $H_2POSH$ started in 1999 the Berlin group, in close cooperation with Fujimura and coworkers in Sendai (Japan). Together [182], they performed the first quantum model simulation of the selective preparation of enantiomers by means of optimal, elliptically polarized, infrared picosecond laser pulses. The simulations were done assuming a preoriented model system and the optimal field was obtained by means of local optimal control theory, cf. Ref. [186, 187, 188]. The underlying mechanism to convert 50%:50% racemic mixture into a pure enantiomer (100%:0%) involves sequential transitions between the two lowest doublets of delocalized eigenstates with different + and - symmetries, respectively.

Moreover, it was demonstrated that also linearly polarized laser field can be used to convert a racemate into a pure enantiomer [89, 90]. The low temperature limit was considered in the simulations to make sure that only the lowest doublet of the torsional states are populated. The suggested strategy [89] employs five laser pulses in the infrared domain to convert the initial state, an incoherent superposition of states representing enantiomers with opposite chiralities, to the final state, an incoherent superposition of two coherent states (a single enantiomer).

González et al [189], starting from the obtained optimal control pulses, could design various series of pump-dump laser pulses with analytical shapes for the

preparation of a single enantiomer, starting from a coherent superposition of preoriented, left and right atropisomers in the electronic and torsional ground state. Various scenarios of sequential elliptically and/or linearly polarized laser pulses were developed, based on the analysis of the original optimal laser pulse, its resulting population dynamics and the symmetry selection rules for the laser induced transitions. Interestingly, for each of the different scenarios, the left or right enantiomer can be prepared selectively by either changing the corresponding left to right polarization of the elliptical pump and/or dump pulses or using corresponding 180° phase-shifts of the equivalent linear polarized laser pulses.

A different selective preparation of enantiomers from preoriented $H_2POSH$ at low temperature was presented by Hoki and coworkers [91] using a one dimensional model and optimal control theory. The optimal electric field consisted of a sequence of two infrared linearly polarized pulses with the same phases but with different magnitudes. The optimal electric field transfers the L-form into the R-form while suppressing the reverse process. A two dimensional model including the free rotation around the preoriented torsional axis was considered in Ref. [190]. Here the selective preparation of enantiomers was controlled by a sequence of infrared circularly polarized pulses.

A considerably faster time scale was achieved exchanging the infrared five linearly polarized laser pulses by sub-picosecond and UV only [92]. Two strategies were proposed, one using so called $\pi$-pulses, cf. [191], and another one using chirped or adiabatic pulses.

In contrast to previous approaches, which employed at least four pulses, Hoki and coworkers suggested a series of just two selective intense polarized laser pulses which transform an oriented, non-rotating racemate into pure enantiomers [192]. The first ”pump” pulse excites exclusively the undesired enantiomer into an excited, delocalized state. The second ”dump” pulse transforms this excited state into a localized excited state of the target enantiomer. The pulses can involve infrared transitions, like in [192], or electronic excited state transitions [193]. The fundamental principle is to adjust the photon polarizations of the pulses in such a way that there is a large interaction between the laser and one of the enantiomers, while the interaction with the other enantiomer vanishes. A pump and dump lasers with $\pi$-pulse area are used to produce the maximum transfer yield of the molecular handedness.

An important step is made in Ref. [94] where Hoki and coworkers presented control of molecular handedness in a randomly oriented racemic mixture using

three polarization components of electric field [194]. One of the three polarization components is used for orientation of the molecule and then the other two components are used for controlling chirality using the pump-dump mechanism.

STImulated Raman Adiabatic Passage (STIRAP) method [195] has been applied to population transfer in a degenerated system [93]. Pure state and mixed state have been taken into account. For the pure state case, a STIRAP with a linearly polarized single laser allows an almost complete population transfer from one enantiomer to the other by adiabatically changing its polarization direction. For the mixed state, a STIRAP with two linearly polarized laser pulses allows a selective preparation of pure enantiomer from a racemate, see also Ref. [92].

## 4.2 Selection of coordinates

The quantum dynamical simulation will be demonstrated, as we mentioned in section 4.1, for the deuterated phosphinothioic acid ($H_2POSD$) which presents (transient) axial chirality. The molecule is considered to be in the "old, molecular" frame (x,y,z) with the atom P at the origin, the OPS fragment in the x/z-plane and the O atom in the positive direction of the x-axis; the P-S bond is along the z-axis and it is denoted by $r$. The chiral coordinate is the OPSD torsional angle $\phi$ around the z-axis, see Fig. 4.4a. In the simulations, one can also consider the system in the "new, laboratory" frame (X,Y,Z) with orientation as shown in Fig. 4.4b. Here the center of mass (c.o.m) of $H_2PO$ is considered as the origin, the positive direction of the Z-axis is passing through the c.o.m of the SD fragment, the O atom lies in the negative direction of X-axis, $r'$ is the distance between c.o.m of $H_2PO$ and that of SD and $\phi'$ is the relative rotation of SD with respect to $H_2PO$, i.e. the angle between the planes OPS and DSP.

The principle coordinate which should be considered is the torsional angle $\phi/\phi'$ since this is the coordinate responsible for the interchange of molecular chirality. Upon ultraviolet (UV) irradiation, the molecule undergoes P-S bond fragmentation. As we will show later, one can make use of this photo-fragmentation to eliminate one of the enantiomers and keep the other one. The coordinate describing dissociation is the P-S bond, $r/r'$. Therefore the relevant coordinates are the $r$ and $\phi$ or equivalently $r'$ and $\phi'$. The subsequent quantum chemical calculations generate the potential energy surfaces and dipole surfaces in terms of $r$ and $\phi$. In contrast, the coordinates $r'$ and $\phi'$ are employed to simplify the Hamiltonian used in the simulation of the laser driven dynamics, i.e. because the kinetic cou-

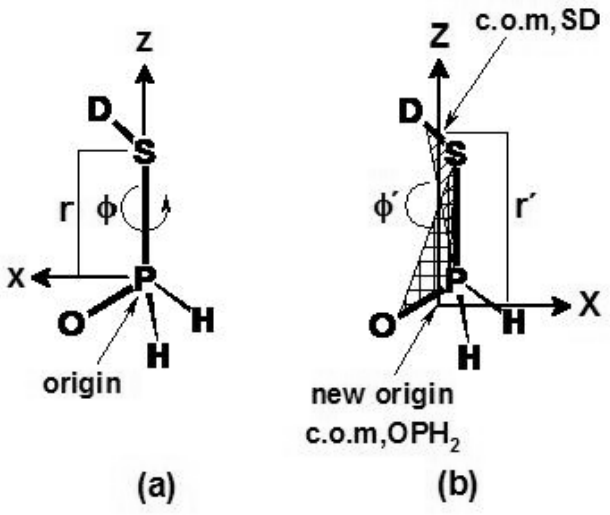


Figure 4.4: Molecular orientation of $H_2POSD$: (a) Shows the molecule fixed coordinates $r$ and $\phi$, which describe the P-S distance and the torsional angle OPSD, respectively. (b) Shows the laboratory coordinates $r'$ and $\phi'$, which describe the distance between the centers of masses of the SD and $H_2PO$ fragments, and the corresponding torsional motion between them, respectively

pling vanishes for those coordinates; for the coordinate transformation see section 4.4 and Appendix D. The remaining degrees of freedom are kept frozen at the equilibrium geometry.

## 4.3 The electronic structure of $H_2POSD$

The model system, $H_2POSD$, is assumed to be oriented before the optical separation of enantiomers takes place. As mentioned in section 4.2, the molecule is oriented such that the P-S bond is along the positive direction of the z-axis and the SPO atoms are in the x/z-plane with O atom directed to the positive x-axis, Fig. 4.4a. The chiral coordinate $\phi$ is the torsional motion of the D atom around the P-S bond. The coordinate $\phi$ is considered as $0^\circ$ when the D atom is in the x/z-plane and directed towards the positive x-axis. On the other hand, $\phi$ becomes $180^\circ$ when the D atom is in the x/z-plane and directed to the negative x-axis upon rotation of the D atom around the P-S bond in certain direction, and $\phi$ becomes $-180^\circ$ when the D atom is in the x/z-plane and directed to the negative x-axis upon rotation of the D atom around the P-S bond in the reverse direction. The molecular geometry of the $H_2POSD$ (Fig. 4.2), taken from Ref. [182], was fully optimized using the

gradient minimization technique with MP2 at the 6-311+G(2d,p) level of theory as implemented in the Gaussian98 program package [154]. The global minimum is characterized by having zero gradient norms and by positive eigenvalues when diagonalizing the matrix of the second derivatives. The bond lengths and the bond angles of the equilibrium geometry are shown in table (4.1).

For one enantiomer, the dihedral angle (OPSH), which governs the axial chirality, is 59.5° at equilibrium. This non-zero angle makes the two P-H bonds slightly different, i.e. the P-H bond which is in the same direction of the S-H bond is slightly smaller than the one in the opposite direction. On the other hand, the situation is reversed for the other enantiomer. In the calculation of the potentials and other properties, the two P-H bonds are averaged to be 1.4Å and therefore, the molecule has $C_s$ symmetry in case of 0° OPSH dihedral angle.

| Label | Bond length (A) | Label | Bond angle (°) |
|---|---|---|---|
| P-S | 2.115 | $\angle(PSH)$ | 93.2 |
| P-O | 1.478 | $\angle(OPS)$ | 118.8 |
| P-$H_a$ | 1.399 | $\angle(H_bPO)$ | 116.6 |
| P-$H_b$ | 1.397 | $\angle(H_aPS)$ | 96.9 |
| S-H | 1.337 | | |

Table 4.1: The bond lengths (A) and bond angles (°) of the equilibrium geometry of $H_2POSH$ calculated at the MP2/6-311+G(2d,p) level [182].

## 4.4 The two dimensional (2D) Hamiltonian

The quantum chemical calculations of the two-dimensional model system employ the torsional angle of S-D around the P-S bond ($\phi$) and the P-S stretch ($r$), while the other degrees of freedom are kept fixed at their equilibrium values. If one employs the same coordinates for the quantum dynamical simulations (neglecting non-adiabatic couplings), then the Hamiltonian consists of the potential energy term ($\vec{V}(r,\phi)$), which will be discussed in section 4.5, the kinetic energy operator ($\hat{T}(r,\phi)$) plus a term $\hat{T}_{coupling}$ for the kinetic couplings of the $r$ and $\phi$ degrees of freedom, and a coupling term ($-\vec{\mu}_{ij}\vec{\epsilon}(t)$), which describes the interaction with laser radiation in the semiclassical dipole approximation. The transition dipole moment vector between the $i$ and $j$ states is given by $\vec{\mu}_{ij} = \vec{\mu}_{ji}$, and $\vec{\epsilon}(t)$ is the electric field vector specified in equation (2.107). Then, the Hamiltonian in inter-

nal bond-angle coordinates, $r$ and $\phi$, looks like:

$$\begin{aligned}\hat{H}(r,\phi) &= \hat{T}(r,\phi) + \hat{V}(r,\phi) - \vec{\mu}_{ij}\vec{\epsilon}(t) \\ &= -\frac{\hbar^2}{2m}\frac{\partial^2}{\partial r^2} - \frac{\hbar^2}{2I}\frac{\partial^2}{\partial \phi^2} + \hat{T}_{coupling} + V(r,\phi) - \vec{\mu}_{ij}\vec{\epsilon}(t),\end{aligned} \tag{4.1}$$

where $m$ is an effective reduced mass of the S and P atoms, and $I$ is an effective moment of inertia of the dihedral rotation of the frozen fragments SD and $OPH_2$ around the P-S bond.

For the sake of avoiding the coupling term ($\hat{T}_{coupling}$) in the dynamical simulations, instead of the internal bond-angle coordinates $r$ and $\phi$, one can use $r'$ and $\phi'$, see Fig. 4.4b, for which the kinetic couplings vanish (for more details see Appendix D). Now, analogously to the situation of having two non-linear interacting molecules [196], $H_2POSD$ is considered to be composed of two fragments: the $H_2PO$ fixed in the space and the SD rotating around an axis connecting the center of masses of these two fragments. The positive direction of the Z-axis passes from the center of mass, c.o.m, of the rigid part $OPH_2$ to the c.o.m of the other rigid part SD. Then, the transformed coordinate $r'$ is given by the distance between the c.o.m of both fragments, and $\phi'$ is the relative rotation of SD with respect to $OPH_2$ or the angle between the planes OPS and DSP (see Fig. 4.4b). Using these new coordinates, $r'$ is decoupled from other degrees of freedom, and it is possible to write the kinetic energy operator as [196]:

$$\hat{T}'(r',\phi') = \frac{-\hbar^2}{2m'}\frac{\partial^2}{\partial r'^2} + \frac{-\hbar^2}{2I'_{SD,OPH_2}}\frac{\partial^2}{\partial \phi'^2}, \tag{4.2}$$

with $m'$ is the reduced mass of the SD and $OPH_2$ fragments,

$$m' = \frac{m_{SD}m_{OPH_2}}{m_{SD}+m_{OPH_2}}. \tag{4.3}$$

and $I'_{SD,OPH_2}$ is the reduced moment of inertia, see Appendix E,

$$I'_{SD,OPH_2} = \frac{I_{SD}I_{OPH_2}}{I_{SD}+I_{OPH_2}}. \tag{4.4}$$

The corresponding potential energy surfaces $V_i'$ and transition dipole surfaces $\vec{\mu}'_{01}$ are then calculated from the original $V_i$ and $\vec{\mu}_{01}$ as described in Appendix D.

## 4.5 Potential energy surfaces and dipole moments

The electronic ground and first excited singlet potential energy surfaces, $V_0(r,\phi)$ and $V_1(r,\phi)$, are the basis for constructing the molecular Hamiltonian, as discussed in the previous section. The unrelaxed electronic ground $V_0(r,\phi)$ and first

excited singlet state $V_1(r,\phi)$ potential energy surfaces (Fig. 4.5a,b) have been calculated using the ab initio multiconfigurational method of complete active space self-consistent field (CASSCF) [197], as implemented in the MOLCAS4.3 quantum chemical software package [198]. Except for $r$ and $\phi$, all the geometrical parameters are frozen at their equilibrium geometry. Because the ground and the excited states are degenerate at the asymptotic region, both roots have been calculated with state averaging (SA) of equal weights. The active space considered is 14 electrons correlated in 12 active orbitals, including the lone pairs of oxygen and sulfur atoms, the bonding/antibonding $\sigma/\sigma^*$ pairs of the P-S and P=O bonds, and Rydberg orbitals. Within such active space, the lowest singlet state was found to be mainly a HOMO-LUMO transition, exciting an electron from the lone pair of the S atom to an antibonding P-S orbital ($n_S$-$\sigma^*_{P-S}$ excitation). The SA-CASSCF calculations were made with the ANO-L basis set of the size (17s12p5d) primitives contracted to [4s3p2d] for the P- and S-atoms, (14s9p4d) contracted to [4s3p2d] for the O-atom, and (8s4p) contracted to [3s2p] for the H-atoms, summing to a total number of 114 contracted basis functions. The electronic transition dipole moment surfaces have been obtained at the same level of theory as the PES.

The PES $V_0$ in the electronic ground state $S_0$ has two stable configurations at ($\phi, r$) = ($-1.0rad, 4.1a_o$) and ($1.0rad, 4.1a_o$) which correspond to L and R enantiomers of the $H_2$POSD molecule, respectively. There exist a transition state at ($\phi, r$) = ($0.0rad, 4.1a_o$), with a barrier height of ca. 400 $cm^{-1}$. In contrast, the singlet excited state $S_1$ surface is repulsive along the P-S bond coordinate and therefore does not have any stable configuration at the employed level of theory, see Fig. 4.5a,b. The Franck-Condon vertical excitation energy at the (L) or (R) configurations is 5.81 eV. The repulsive character of the PES $V_1$ along the P-S bond stems from the main configuration ($n_S$-$\sigma^*_{P-S}$) contributing to the first excited singlet state, in which an electron is promoted to an antibonding orbital. The x, y and z components of the transition dipole surfaces $\vec{\mu}_{01}(r,\phi)$ are shown in Fig. 4.6a,b,c. The x and z components are anti-symmetric with respect to $\phi$ while the y component is symmetric.

As has been discussed in section 4.4 the kinetic energy operator has a complex form in terms of these internal coordinates. For the sake of simplicity one can transform the internal coordinates $r$ and $\phi$ into others whose kinetic energy operator has a simpler form, i.e. the kinetic coupling is negligible, see Appendix D. The torsional angle $\phi$ does not change for large values of $r'$ and $\phi'$ upon transfor-

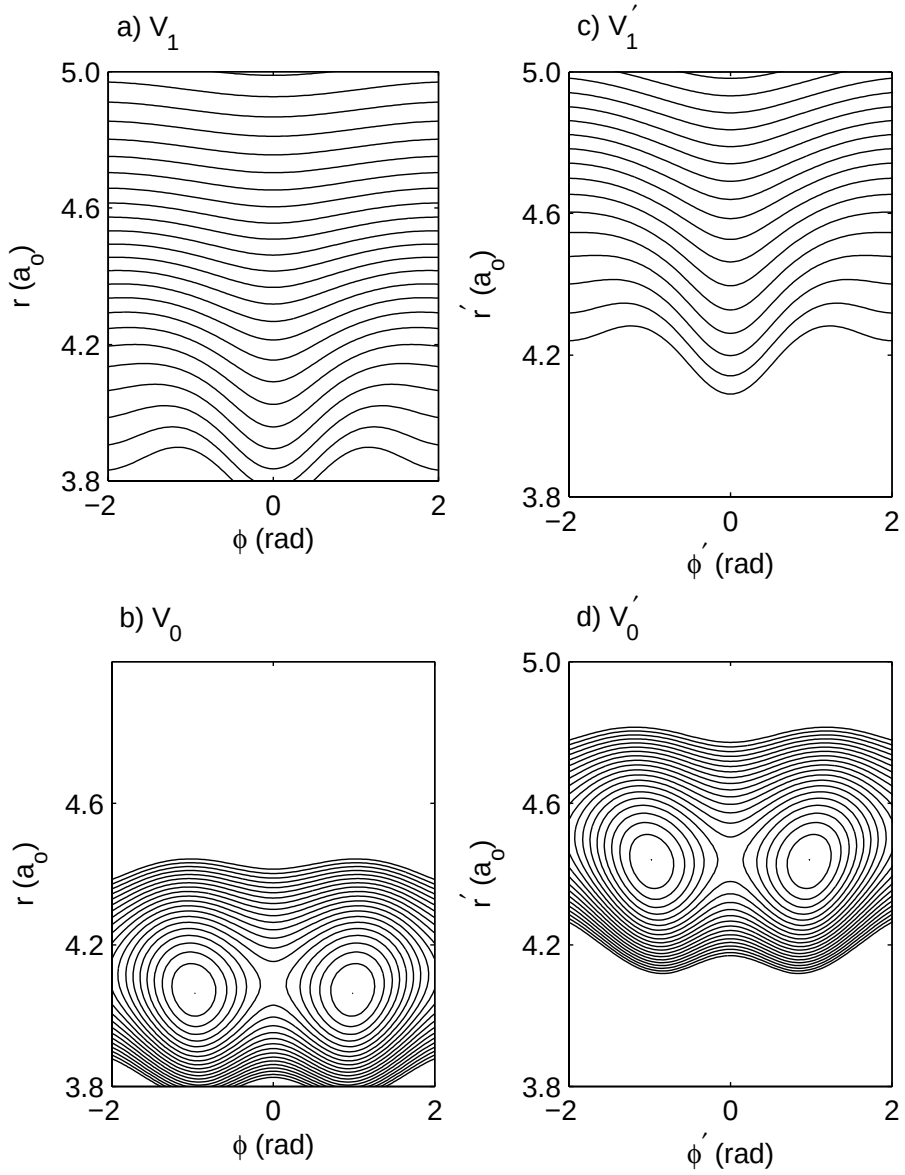


Figure 4.5: Contour plots of the potential energy surfaces of $H_2$POSD calculated at SA-2-CASSCF(14,12) level of theory as a function of the torsion angle $\phi$ (in radians) and the distance $r$ (in $a_0$) between the fragments $H_2$PO and SD. Panels (a)/(c) and (b)/(d) are for the first electronic singlet excited state $V_1/V_1'$ ($S_1$) and the electronic ground state $V_0/V_0'$ ($S_0$), respectively. The contour lines are drawn from 0.01 eV until 0.2 eV at regular intervals of 0.01 for $V_0$; and from 3 eV until 6.2 eV at regular intervals of 0.1 for $V_1$; the zero energy is located at the minimum of the $S_0$ surface.

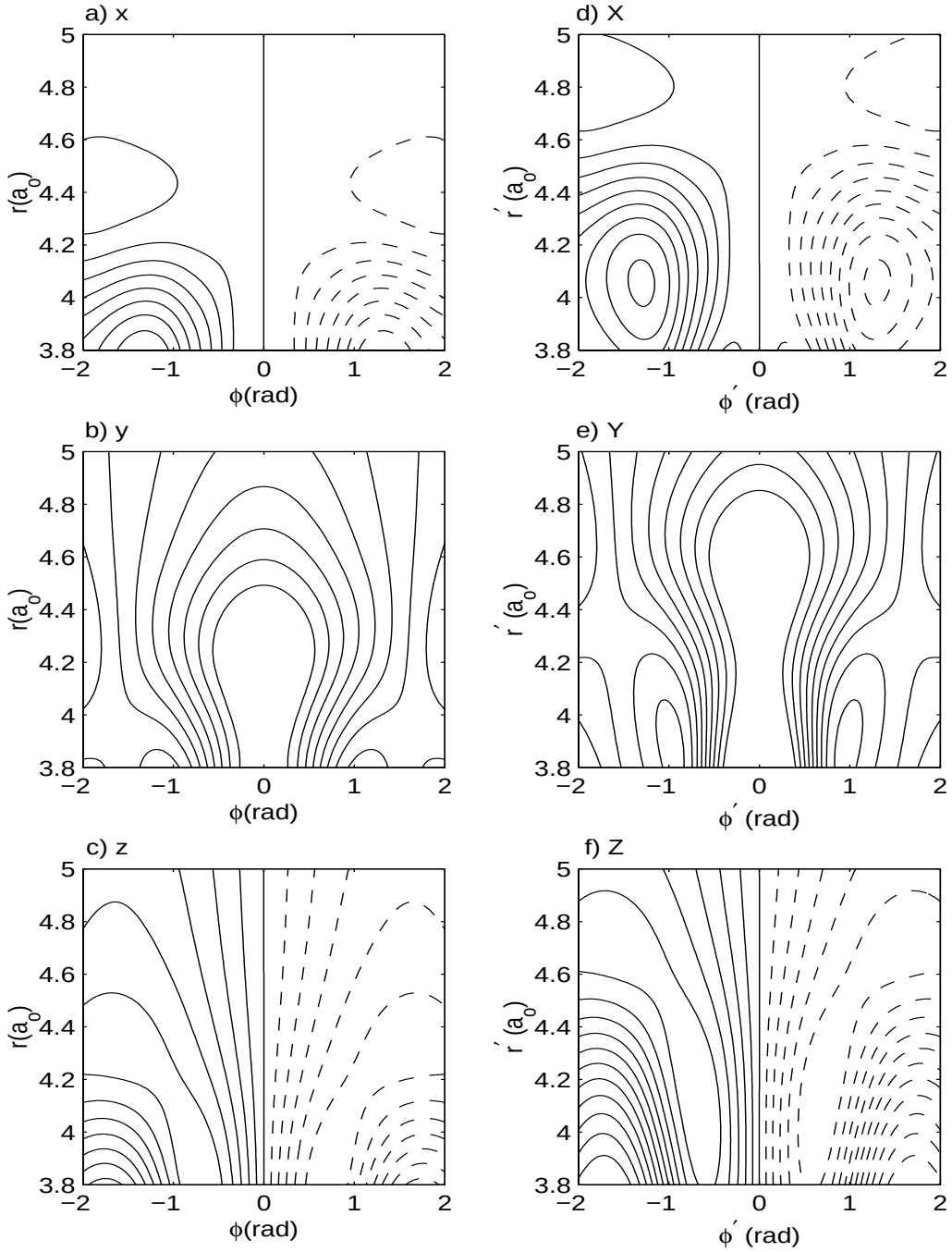


Figure 4.6: Contour plots of the x- (a), y- (b), z- (c), X- (d), Y- (e) and Z- (f) components of the transition dipole moment of $H_2$POSD, as a function of the torsion angle $\phi$ (in radians) and the distance $r$ (in $a_0$) between the fragments $H_2$PO and SD. The lines are drawn from -0.08 to 0.08 in intervals of 0.01 for the x-/X-component, from -0.06 to 0.06 in intervals of 0.01 for the y-/Y-component and from -0.05 to 0.05 in intervals of 0.01 for the z-/Z-component (in e $a_0$).

mation from old coordinates to new ones. Moreover, distance $r$ does not change much upon transformation for large values of $r'$ and $\phi'$, see Fig. 4.7. As shown in Fig. 4.7 (top), the vertical lines are tilted for small values of $r'$ and $\phi'$, while they become straight for larger values of $r'$ and $\phi'$. Further, the horizontal lines are a bit curved around $\phi'$ = 0 and small values of $r'$, while they become straight for larger values of $r'$ along $\phi'$ as shown in Fig. 4.7 (bottom).

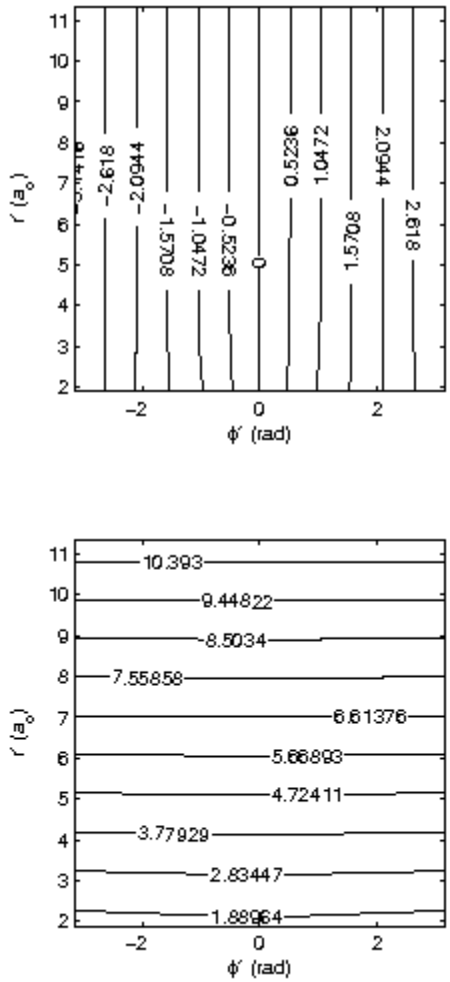


Figure 4.7: Contour plots of $\phi$ versus the new coordinates, $\phi'$ and $r'$, (upper panel) and $r$ versus the new coordinates, $\phi'$ and $r'$, (lower panel).

From this coordinate transformation one can get the potential energy surfaces in terms of the new coordinates $r'$ and $\phi'$ as shown in Fig. 4.5c,d. Also, one can get the X, Y and Z components of the transition dipole moments in terms of the new coordinates $r'$ and $\phi'$ as shown in Fig. 4.6d,e,f. Therefore, the new potential energy surfaces, in the new coordinates, as well as the new transition

dipole moments, in the new coordinates, can be used in the quatum dynamical simulations.

## 4.6 Vibrational eigenfunctions

Having defined the 2D-Hamiltonian using the calculated potential energy surfaces, one can solve the time independent nuclear Schrödinger equation, Eq. (2.18), to get the vibrational eigenfunctions. For this purpose, one may use the Fourier-Grid-Hamiltonian technique [132, 131] discussed in section 2.4.1. A space discretization of 256 grid points for the dissociation degree of freedom $r'$ and 32 grid points for the chiral coordinate $\phi'$ were used making a total of 8192 grid points. The vibrational eigenfunctions are calculated using the QMBOUND program implemented in the WAVEPACKET package [199]. These vibrational eigenfunctions are calculated for the electronic ground state $S_0$ potential energy surface which is a bound state. On the other hand, the electronic excited state $S_1$ is repulsive and has no stable configuration in the electronic excited state, therefore one can not calculate bound vibrational eigenfunctions. The lowest 18 eigenfunctions and the corresponding eigen-energies for the electronic ground state $S_0$ are shown in Table 4.2.

The lowest eigen-energies appear in doublets due to the splitting resulting from the potential barrier at $\phi'$ = 0° which separates the two minima. In the electronic ground state $S_0$, there are three doublets ($v$ = 0,1,2), under the barrier, corresponding to the eigenvalues $E_{0,wv+/-}$ and eigenfunctions $\psi_{0,wv+/-}$ with + and - depending on their symmetry with respect to reflection at $\phi$ = 0°. Here $w$ represents the quantum number corresponding to the stretching degree of freedom $r'$ and $v$ represents the quantum number corresponding to the torsional degree of freedom $\phi'$. The subscript 0 indicates the electronic ground state $S_0$. Since the energy gaps between the eigenstates for the stretching coordinate is quite large, the first vibrational excited stretching mode appears after four doublets of torsional modes, see Table 4.2. The vibrational eigenfunctions $\psi_{0,00+}$, $\psi_{0,00-}$, $\psi_{0,10+}$, $\psi_{0,10-}$, $\psi_{0,11+}$ and $\psi_{0,11-}$ are shown in Figs. 4.8(a-f), respectively.

| Eigenfunction | Eigenvalue (eV) |
|---|---|
| $\psi_{0,00+}$ | $2.9477 \cdot 10^{-02}$ |
| $\psi_{0,00-}$ | $2.9479 \cdot 10^{-02}$ |
| $\psi_{0,01+}$ | $4.7586 \cdot 10^{-02}$ |
| $\psi_{0,01-}$ | $4.7665 \cdot 10^{-02}$ |
| $\psi_{0,02+}$ | $6.3044 \cdot 10^{-02}$ |
| $\psi_{0,02-}$ | $6.4121 \cdot 10^{-02}$ |
| $\psi_{0,03+}$ | $7.4889 \cdot 10^{-02}$ |
| $\psi_{0,03-}$ | $7.9672 \cdot 10^{-02}$ |
| $\psi_{0,10+}$ | $8.0212 \cdot 10^{-02}$ |
| $\psi_{0,10-}$ | $8.0258 \cdot 10^{-02}$ |
| $\psi_{0,04+}$ | $8.7952 \cdot 10^{-02}$ |
| $\psi_{0,04-}$ | $9.5411 \cdot 10^{-02}$ |
| $\psi_{0,11+}$ | $9.8215 \cdot 10^{-02}$ |
| $\psi_{0,11-}$ | $9.8437 \cdot 10^{-02}$ |
| $\psi_{0,05+}$ | $1.0350 \cdot 10^{-01}$ |
| $\psi_{0,05-}$ | $1.1077 \cdot 10^{-01}$ |
| $\psi_{0,12+}$ | $1.1340 \cdot 10^{-01}$ |
| $\psi_{0,12-}$ | $1.1493 \cdot 10^{-01}$ |

Table 4.2: The eigenvalues (in eV) corresponding to the first eighteen eigenfunctions in the electronic ground state $V_0$. Subindices indicate the quantum numbers corresponding to the electronic state (in this case, ground state), the stretching degree of freedom $r'$, the torsional degree of freedom $\phi'$ and symmetry.

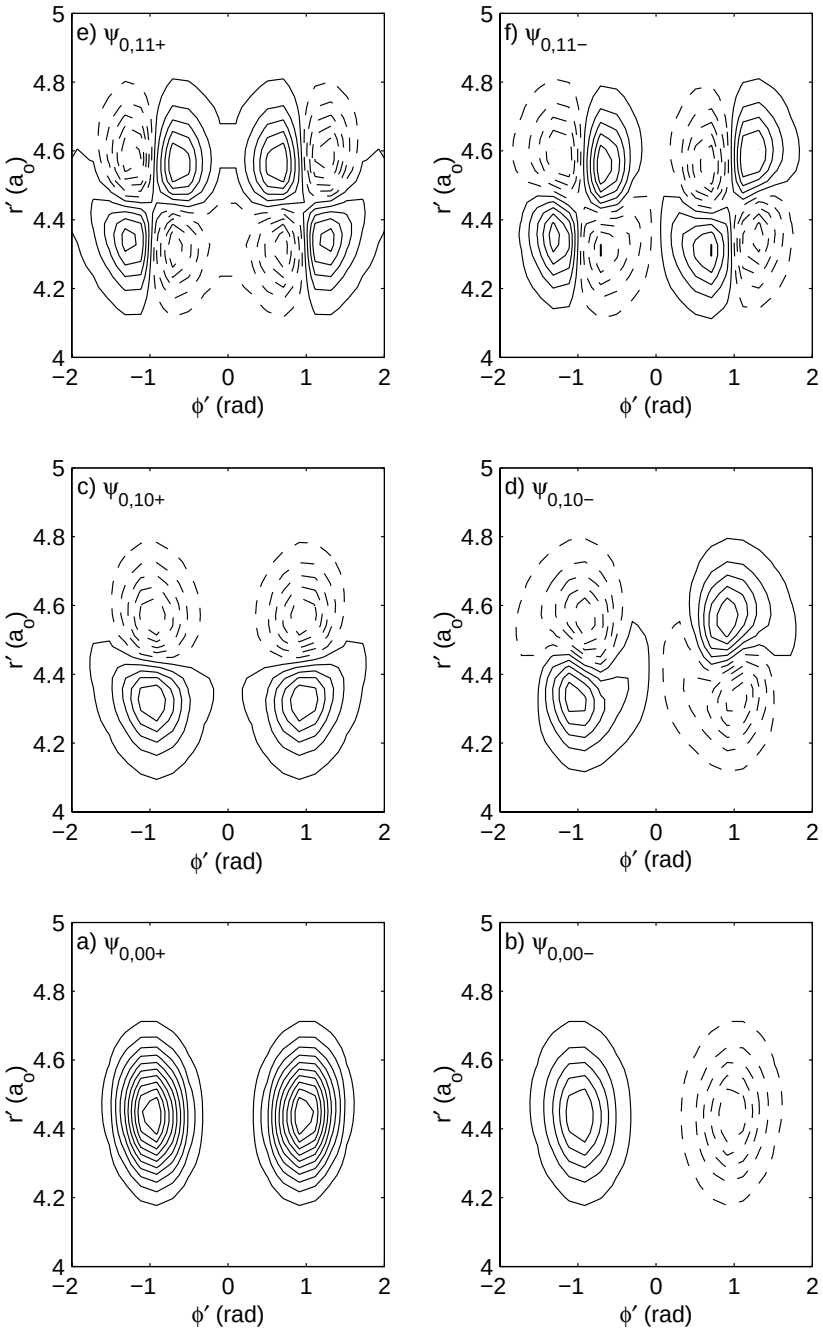


Figure 4.8: The two dimensional eigenfunctions calculated in the electronic ground state ($S_0$) of $H_2$POSD with + or - symmetries with respect to inversion at $\phi'$ = 0°: a) $\psi_{0,00+}$ ; b) $\psi_{0,00-}$ ; c) $\psi_{0,10+}$ ; d) $\psi_{0,10-}$ ; e) $\psi_{0,11+}$ ; f) $\psi_{0,11-}$. The corresponding eigenenergies are shown in Table 4.2.

The pure L-/R-enantiomers are represented by the localized wave functions $\psi_{0,wvL/R}$ embedded in the left and the right potential minima with respect to $\phi'$ = 0° of the electronic ground state $S_0$. They are constructed as superpositions of two eigenstates in the electronic ground state $S_0$ ($\psi_{0,wv+}$ and $\psi_{0,wv-}$) with different parities [69] as shown in Fig. 4.9.

$$\psi_{0,wvL} = \frac{1}{\sqrt{2}}\Big(|\psi_{0,wv+}\rangle + |\psi_{0,wv-}\rangle\Big) \tag{4.5a}$$

$$\psi_{0,wvR} = \frac{1}{\sqrt{2}}\Big(|\psi_{0,wv+}\rangle - |\psi_{0,wv-}\rangle\Big). \tag{4.5b}$$

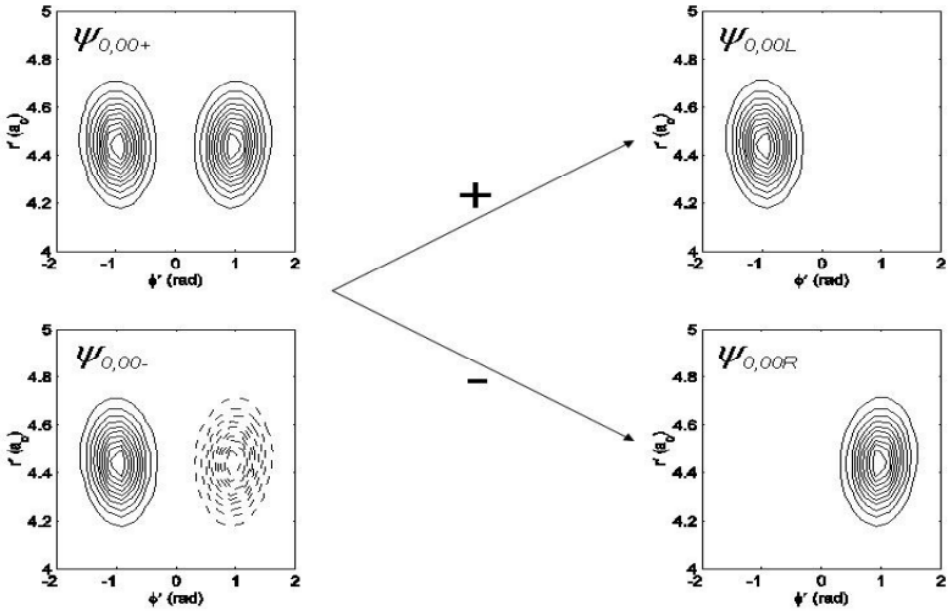


Figure 4.9: The two dimensional localized wave functions for the left ($\psi_{0,00L}$) and right ($\psi_{0,00R}$) enantiomers of $H_2$POSD as defined in Eqn. (4.5). These wave functions are calculated for the first doublet, $\psi_{0,00+}$ and $\psi_{0,00-}$ (Figs. 4.8a and 4.8b, respectively), in the electronic ground state.

The energy splittings, $\Delta E_{0,v}$, of the first three doublets under the barrier are calculated and collected in Table 4.3 with the corresponding tunneling time. The tunneling time, $\tau$, is defined as the whole oscillation period L-R-L and is inversely proportional to the energy splitting:

$$\tau_v = \frac{h}{\Delta E_{0,v}}. \tag{4.6}$$

As shown in Table 4.3 the energy splittings increase with increasing energy where the potential barrier gets tighter allowing more interaction between the eigenstates in each well.

| Doublet | $\Delta E_v^0$ (cm$^{-1}$) | $\tau_v$ |
|---|---|---|
| 0+/0- | 0.02 | 1.8 ns |
| 1+/1- | 0.64 | 51.6 ps |
| 2+/2- | 8.69 | 3.8 ps |

Table 4.3: The energy splittings (in cm$^{-1}$) of the first three doublets and the corresponding tunneling times for the model $H_2$POSD.

In order to keep enantiomer selectivity and have enough time to further treat the separated enantiomer, the laser pulse duration should be much shorter than the tunneling time. This is an important criterion which should be fulfilled. In the next section we will see how to separate enantiomers in an pre-oriented racemate using photo-dissociation.

## 4.7 Separation of enantiomers in a pre-oriented racemate

The laser-driven time evolution of the system is simulated by means of molecular wave packets, calculated as solutions of the Liouville-von Neumann equation, Eqn. (2.131), for the time-dependent density matrix $\rho(t) = |\psi(t)\rangle\langle\psi(t)|$, see section 2.5. The total Hamiltonian $\hat{H}(t)$ is written as $\hat{H}(t) = \hat{H}_{mol} + \hat{W}(t) = \hat{T}+\hat{V}+\hat{W}(t)$. The laser field $\hat{W}(t)$ should be tailored to excite a single enantiomer from the initial racemic state, which is given by,

$$\rho(t=0) = \rho_{rac}(T) \tag{4.7}$$

which represents a racemic mixture at temperature T. Considering the limit of low T, the initial racemic mixture can be written as an incoherent superposition of the lowest doublet of eigenstates [89]: (cf. Eqs. (2.128) and (2.129))

$$\rho_{rac}(T \to 0) \approx \frac{1}{2}|\psi_{0,00+}\rangle\langle\psi_{0,00+}| + \frac{1}{2}|\psi_{0,00-}\rangle\langle\psi_{0,00-}|, \tag{4.8}$$

where $|\psi_{0,00+}\rangle$ and $\langle\psi_{0,00-}|$ states are the vibrational eigenfunctions in the electronic ground state obtained as solutions of the time independent Schrödinger equation, Eq. (2.9), with symmetry + or - for the torsional motion (see Table 4.2).

Equation (4.8) can be also written in terms of the localized states as follows:

$$\rho_{rac}(T \to 0) \approx \frac{1}{2}|\psi_{0,00L}\rangle\langle\psi_{0,00L}| + \frac{1}{2}|\psi_{0,00R}\rangle\langle\psi_{0,00R}|, \tag{4.9}$$

where $|\psi_{0,00L}\rangle$ and $\langle\psi_{0,00R}|$ correspond to L- or R-enantiomers in the lowest doublet states, and in general, are defined as coherent superpositions of the torsional eigenstates of different parity as mentioned in section 4.6 [69] (cf. Eqs. (2.129) and (2.130)). In the absence of dissipation, the laser driven time evolution of a racemic mixture can be described with two independent time-dependent Schrödinger equations for the L and R enantiomers,

$$i\hbar\frac{\partial}{\partial t}\begin{pmatrix} |\psi_{0,00L}(t)\rangle \\ |\psi_{1,00L}(t)\rangle \end{pmatrix} = \begin{pmatrix} \hat{T}_n + V_0 & -\vec{\mu}_{01}\vec{\epsilon}(t) \\ -\vec{\mu}_{10}\vec{\epsilon}(t) & \hat{T}_n + V_1 \end{pmatrix}\begin{pmatrix} |\psi_{0,00L}(t)\rangle \\ |\psi_{1,00L}(t)\rangle \end{pmatrix} \tag{4.10}$$

and

$$i\hbar\frac{\partial}{\partial t}\begin{pmatrix} |\psi_{0,00R}(t)\rangle \\ |\psi_{1,00R}(t)\rangle \end{pmatrix} = \begin{pmatrix} \hat{T}_n + V_0 & -\vec{\mu}_{01}\vec{\epsilon}(t) \\ -\vec{\mu}_{10}\vec{\epsilon}(t) & \hat{T}_n + V_1 \end{pmatrix}\begin{pmatrix} |\psi_{0,00R}(t)\rangle \\ |\psi_{1,00R}(t)\rangle \end{pmatrix}. \tag{4.11}$$

At initial time, t=0,

$$\begin{pmatrix} |\psi_{0,00L}(t)\rangle \\ |\psi_{1,00L}(t)\rangle \end{pmatrix} = \begin{pmatrix} |\psi_{0,00L}(0)\rangle \\ 0 \end{pmatrix} \tag{4.12}$$

$$\begin{pmatrix} |\psi_{0,00R}(t)\rangle \\ |\psi_{1,00R}(t)\rangle \end{pmatrix} = \begin{pmatrix} |\psi_{0,00R}(0)\rangle \\ 0 \end{pmatrix}. \tag{4.13}$$

In order to design a laser pulse which selects a single enantiomer out of an oriented racemic mixture, the direction of the polarization vector of the laser field has to be chosen conveniently [193, 94]. Specifically, excitation of a selected enantiomer will be suppressed if the electric field is perpendicular to the corresponding dominant transition dipole matrix element. In contrast, the interaction for the opposite enantiomer can be maximized if these two vectors are parallel [193, 94]. For instance, to excite the R enantiomer, but not the L one, to some final vibronic eigenfunction $\psi_f$, $\vec{\mu}'_{01}$ and $\vec{\epsilon}(t)$ should satisfy:

$$\begin{aligned} \langle\psi_f|\vec{\mu}'_{01}|\psi_{0,00L}\rangle \cdot \vec{\epsilon}(t) &= 0 \\ \langle\psi_f|\vec{\mu}'_{01}|\psi_{0,00R}\rangle \cdot \vec{\epsilon}(t) &\neq 0 \end{aligned} \tag{4.14}$$

where $\psi_{0,00L}$ and $\psi_{0,00R}$ represent the initial L and R enantiomers defined in eqns. (4.5). In the present molecular system, however, the repulsive excited state potential $V'_1$ does not support any bound eigenfunctions $\psi_f$ but a continuum of states. In the praxis, therefore, the numerical implementation of the rule given in eqn. (4.14) for dissociative states is cumbersome to apply. Instead, let us use an alternative approach. The strategy is shown schematically in Fig. 4.10. The first rectangle in the left hand side represents the symmetric Z-component of the transition dipole

while the second one represents the antisymmetric Y-component of the transition dipole in the dominant domains of the initial wave functions, cf. Fig. 4.6. The sequel rectangle represents the left and right enantiomers. The approximate values of the transition dipole moments in the domain of the wave functions are $\pm 0.04$ for the Z-component and 0.02 for the Y-component, see Fig. 4.10. The idea is to find the values of the amplitude of the laser field (Z- and Y-components) such that the amount of one enantiomer is maximized after its multiplication by the laser field operator with its Z- and Y-components, while that of the other one is minimized after its multiplication by the laser field operator with its Z- and Y-components, see the right hand side of Fig. 4.10. From Fig. 4.10, one can see that the approximate values of the Z-component of the transition dipoles in the domain of the wave functions are twice that of the Y-component of the transition dipoles. Therefore, we started with a field whose Y-component amplitude is twice its Z-component amplitude with different sign. These values can be optimized to get the maximum amount of one enantiomer and minimize the other.

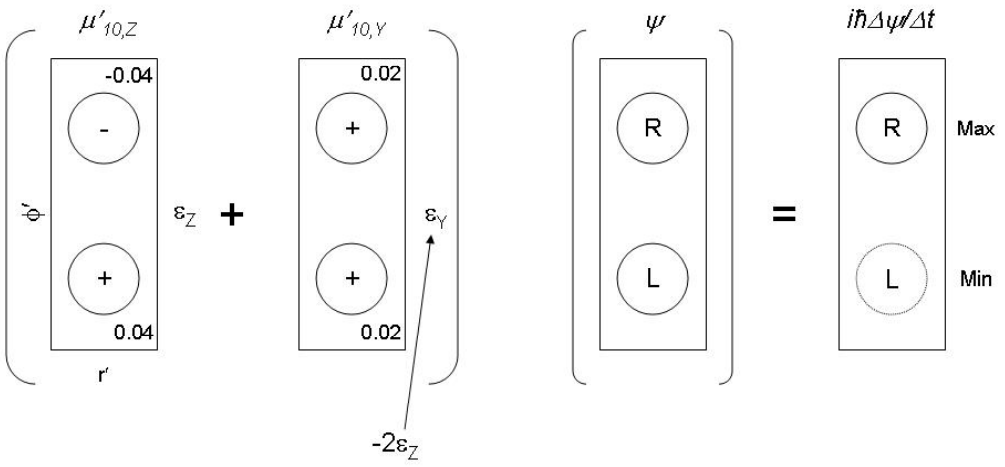


Figure 4.10: Schematic diagram representing the employed strategy for separation of enantiomers via laser pulse control.

Let us consider a scenario where we start from one of the enantiomers, e.g. the R-one, eqn. (4.5b). Using low laser intensities such that the population in $V_1'$ remains small in comparison with the one in $V_0'$ , and inserting eqn. (4.5b) into eqn. (4.11), the change $\Delta\psi_{1,00R} = \psi_{1,00R}(t + \Delta t) - \psi_{1,00R}(t)$ after a small time

step $\Delta t$ is approximately given by,

$$\begin{aligned}\Delta\psi_{1,00R} &\approx -\frac{\Delta t}{i\hbar}\vec{\mu_{10}}\vec{\epsilon}(t)\psi_{0,00R}(t=0) + \frac{\Delta t}{i\hbar}(\hat{T}_n + V_1')\psi_{1,00R}(t) \\ &= \Delta\psi_{1,00R,c} + \Delta\psi_{1,00R,e}. \end{aligned} \tag{4.15}$$

The first term of the right hand side represents the creation (c) of the wave packet in the excited state, while the second one accounts for its evolution (e). Control can be exerted at the time the wave packet is created, and thus, we call this first term $\Delta\psi_{1,00R,c}$, whereas the evolution term is compactly written as $\Delta\psi_{1,00R,e}$. Using two components of the electric field which couple to the symmetric ($\mu_Y'$) and antisymmetric ($\mu_Z'$) components of $\vec{\mu'}$, the control term of eqn. (4.15) can be expanded as,

$$\Delta\psi_{1,00R,c} = -\frac{\Delta t}{i\hbar}(\mu_{10Y}'\epsilon_Y + \mu_{10Z}'\epsilon_Z)\psi_{0,00R}(t=0). \tag{4.16}$$

Similarly,

$$\Delta\psi_{1,00L,c} = -\frac{\Delta t}{i\hbar}(\mu_{10Y}'\epsilon_Y + \mu_{10Z}'\epsilon_Z)\psi_{0,00L}(t=0). \tag{4.17}$$

Then, the ratio between the electric field components $\epsilon_Y$ and $\epsilon_Z$ can be chosen such that the transition dipole interactions ($\mu_{10Y}'\epsilon_Y + \mu_{10Z}'\epsilon_Z$) for example, minimizes the increments $\langle\Delta\psi_{1,00L,c}|\Delta\psi_{1,00L,c}\rangle$, but constructively enhances $\langle\Delta\psi_{1,00R,c}|\Delta\psi_{1,00R,c}\rangle$. This is illustrated in Fig. 4.11. Specifically, Fig. 4.11a and 4.11b show the initial localized wavefunctions $\psi_{0,00L}(t=0)$ and $\psi_{0,00R}(t=0)$, respectively (cf. eqn. (4.5)), Fig. 4.11c and 4.11d show the products $\psi_{0,00L}(t)\mu_Z'\epsilon_Z$ and $\psi_{0,00R}(t)\mu_Z'\epsilon_Z$, and Fig. 4.11e and 4.11f show the analogous products $\psi_{0,00L}(t)\mu_Y'\epsilon_Y$ and $\psi_{0,00L}(t)\mu_Z'\epsilon_Z$, respectively.

Note the different signs of the lobes of the wave function due to the opposite symmetries of $\mu_Y$ and $\mu_Z$. Finally, Fig. 4.11g and 4.11h show the resulting wave functions for $\psi_{0,00L}(\mu_Y'\epsilon_Y + \mu_Z'\epsilon_Z)$ and $\psi_{0,00R}(\mu_Y'\epsilon_Y + \mu_Z'\epsilon_Z)$. The laser parameters used correspond to a linearly polarized laser field with components $\epsilon_Z$ = 2 GV m$^{-1}$ and $\epsilon_Y$ = 1.75 $\mu_Z$. The corresponding maximum intensity is $I_{max}$ = 4.3 TW cm$^{-2}$. Apparently, the increment $\Delta\psi_{1,00L,c}$ is almost negligible while $\Delta\psi_{1,00R,c}$ has been enhanced constructively. Analogous polarizations could be used to minimize $\Delta\psi_{1,00R,c}$ - in this case a field of $\epsilon_Y$ = -1.75 $\epsilon_Z$ would be needed. Therefore, control of the polarization of the electric field allows the excitation of just one enantiomer, whereas the other enantiomer remains in its ground state ($\Delta\psi_{1,00L,c}$ or $\Delta\psi_{1,00R,c}$ = 0).

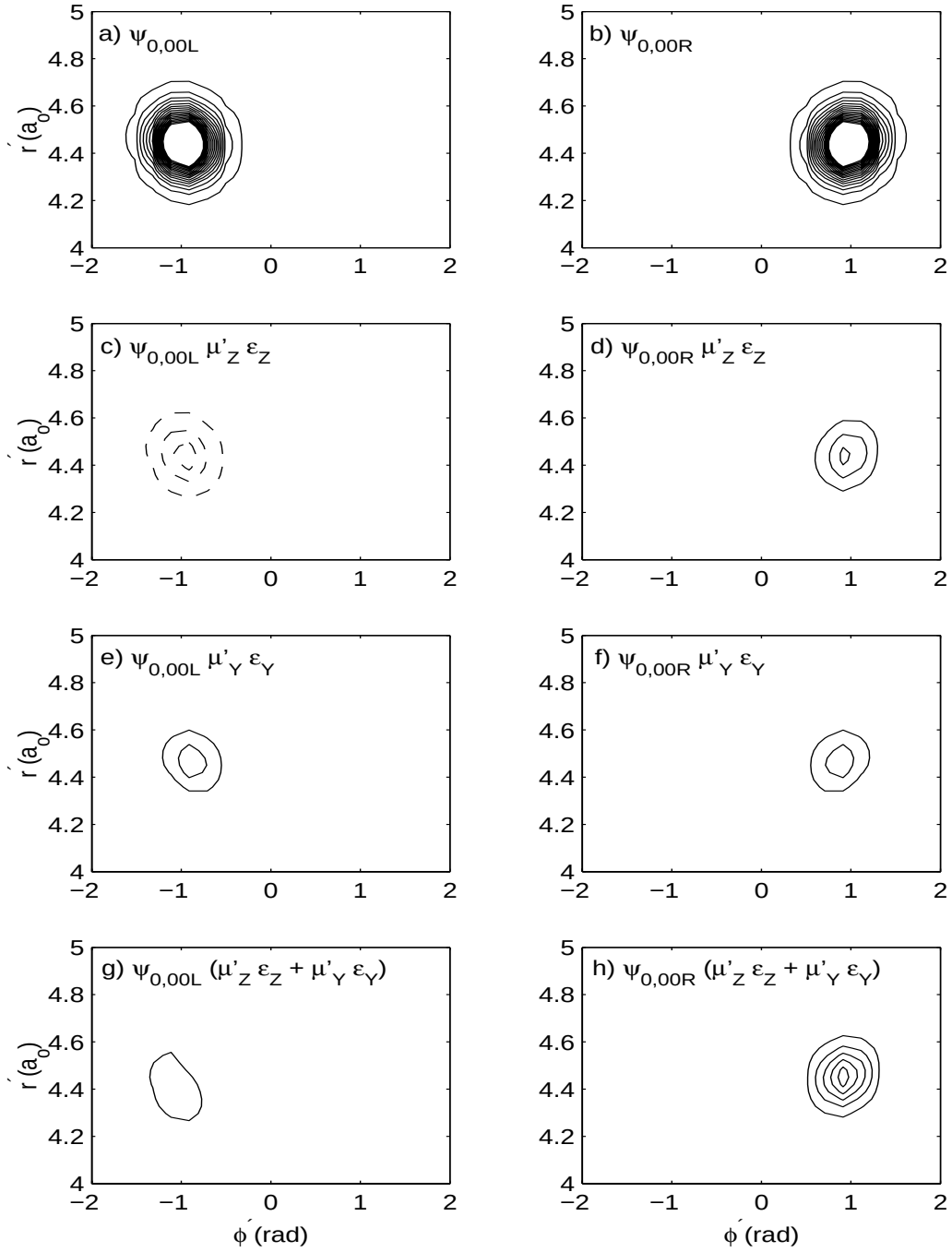


Figure 4.11: Constructive and destructive interferences of the $\psi_{0,00L}(t)$ and $\psi_{0,00R}(t)$ wave functions with transition dipole interactions. The contours in (a) and (b) show the localized $\psi_{0,00L}(t=0)$ and $\psi_{0,00R}(t=0)$ initial wave functions, respectively. The contours in (c) and (d) show the corresponding wave functions after multiplication with the Z-component of the dipole moment (see label), $\epsilon_Z$ = 2 GV m$^{-1}$. The contours in (e) and (f) show the wave functions after multiplication with the Y-component of the dipole moment (see label), $\epsilon_Y$ = 3.5 GV m$^{-1}$. The contours in (g) and (h) show the corresponding wave functions after multiplication with the appropriate sum of dipole interactions (see label).

After having considered the effect of the laser pulse during the time increment $\Delta t$, equivalent to the case of a $\delta$-pulse, one can proceed to apply the strategy described above to excite one enantiomer from a racemic mixture using the entire laser pulse. As an example, the resulting selective photo-excitation of the R-enantiomer from a racemate is demonstrated in Fig. 4.12, showing snapshots of the L and R wave packets in the electronic ground state $S_0$ at $t$ = 0 fs, and in the electronic excited state $S_1$ after 95 fs. The laser parameters obtained in the previous instructive example serve as a reference for the case considered now, i.e. we employ the same laser components, $\epsilon_Z$ = 2 GV m$^{-1}$ and $\epsilon_Y$ = 3.5 GV m$^{-1}$, and the remaining laser parametes are $\omega$ = 5.884 eV, $t_p$ = 100 fs and $\eta$ = 0°. Since the P-S bond breaking occurs on a fs scale, short pulses have been used. The polarization angle resulting from the $\epsilon_Y$ and $\epsilon_Z$ components, which is defined as $\Omega = arctan(\epsilon_Y/\epsilon_Z)$, is 29 °. Due to the weak transition dipole couplings the population excited to the singlet state is about 2%, in accord with the assumption underlying eqn. (4.15); stronger pulses could invert more population to the $S_1$ state. From the excited population, Fig. 4.13 illustrates how the R-enantiomer is successfully excited to the $S_1$ singlet state by a factor of ca. 20 more efficiently than the L-enantiomer, hence demonstrating the selectivity of the applied laser pulses.

The singlet state is strongly repulsive, and therefore, after 95 fs the R-enantiomer has dissociated completely (cf. Fig. 4.12a), never returning back to the reactant in its electronic ground state in gas phase. Notice that the photodissociation path followed by the wave packet is tilted due to the achiral nature of the $S_1$ PES, which possesses a single minimum along the torsional reaction coordinate; as a result the dissociating fragments rotate with respect to each other. By virtue of this ultrafast photodissociation process we have therefore optically resolved the racemic mixture, eliminating the R-enantiomer by a factor of 20 against the L-enantiomer. Similar to the distillation approaches suggested in refs. [81, 200], it should be possible to resolve completely the L-enantiomer from a racemic sample in an iterative manner.

In order to achieve maximum separation, the populations of the L- and R-enantiomers in the electronic excited state can be related to the number of the employed shots by the following equation:

$$\frac{P_R}{P_L} = \frac{(1 - P_f(R))^N}{(1 - P_f(L))^N}, \tag{4.18}$$

where $P_R$ and $P_L$ are the R- and L-enantiomeric populations, respectively; $P_f(R)$,

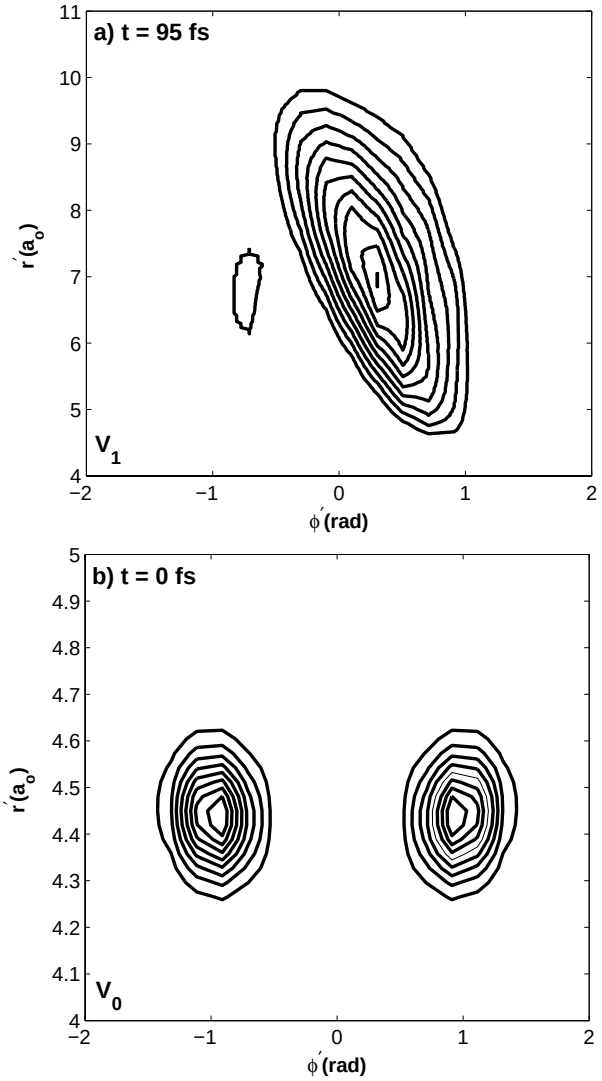


Figure 4.12: Photofragmentation induced in the R-enantiomer of the model $H_2$POSD, while the L-counterpart stays in the electronic ground state $S_0$. (a) Probability density in the $S_1$ state at t = 95 fs. (b) Probability density of the racemic mixture at initial time in the electronic ground state $S_0$.

$P_f(L)$ are the R- and L-enantiomeric populations at the end of the pulse, respectively, and $N$ is the number of the employed shots. Therefore, with the populations of both R- and L-enantiomers at the end of the pulse (Fig. 4.13), one can calculate the number of shots needed to achieve maximum separation. Accordingly, the populations of the L- and R-enantiomers in the electronic excited state obtained from the laser pulses employed imply that ca. 300 shots will be necessary to achieve more than 99% enantiomeric separation, see Fig. 4.14.

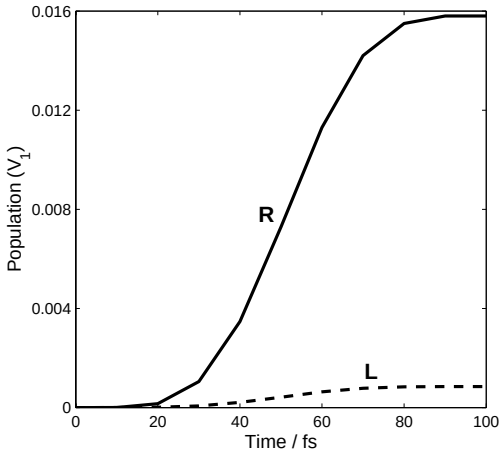


Figure 4.13: Enantiomeric purity as a function of time. The solid line is the population of the R-enantiomer transferred to the dissociative $V_1$ state, the dashed line is the population of the L-enantiomer.

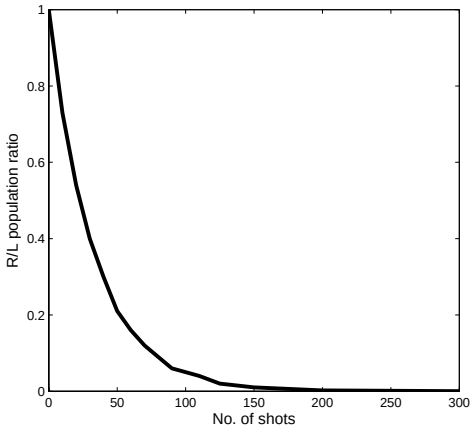


Figure 4.14: The distillation process of R-enantiomer with respect to L-enantiomer after 300 shots. The curve represents a relation between the population ratio (R/L), in $V_1$ state, as a function of number of shots, see Eq. 4.18.